Journal of Materials and Environmental Science
ISSN : 2028-2508
e-ISSN : 2737-890X
CODEN : JMESCN

J. Mater. Environ. Sci., 2026, Volume 17, Issue 8, Page 1343-1355

http://www.jmaterenvironsci.com

Impact of impregnation and activation on the morphological and textural properties of activated carbons derived from *Balanites aegyptiaca* Trunk (BAT)

Oumarou ABDOU GODE[1], Ousmaila SANDA MAMANE[2], Mahamane Nassirou AMADOU KIARI[1,3*], Maman Mousbahou MALAM ALMA[1], Ibrahim NATATOU[1]**

[1]*Department of chemistry, Faculty of Science and Technology, Abdou Moumouni University of Niamey, B.P :10662 Niamey, Niger.*

[2]*Department of fundamental Science, National School of Engineering and Energy Sciences, University of Agadez, B.P: 199 Agadez, Niger*

[3]*Laboratory of Industrial Processes of Synthesis, Environment and New Energies (LAPISEN), National Polytechnic Institute Félix Houphouët-Boigny; BP 1093 Yamoussoukro.*

**Corresponding author, Email address: amadounassirou73@gmail.com*
***Corresponding author, Email address: oumarouabdougode1086@gmail.com*

Received *13 July 2026,*
Revised *20 Aug 2026,*
Accepted *28 Aug 2026*

Citation*: Abdou Godé O., Sanda Mamane O., Amadou Kiari M. N., Malam Alma M. M., Natatou I., (2026) Impact of impregnation and activation on the morphological and textural properties of activated carbons derived from Balanites aegyptiaca Trunk, J. Mater. Environ. Sci., 17(8), 1343-1355.*

Abstract: This present work focused on evaluating the effect of impregnation and activation on the morphological and textural properties of ACs from the trunk of *Balanites aegyptiaca* (TBA). The morphology of the raw BA biomass (BA1) and the AC-BA-20%-450°C was visualized by SEM. The carbon contents evaluated by EDS are 71.89% and 91.28% for the raw BA and AC-BA-20%-450°C, respectively. The activated carbon that developed the best BET specific surface area (393.6 m²/g) is AC-BA-25%-450°C-16h. The prepared activated carbons (ACs) are more thermally stable than the biomass used according to TGA/DSC analyses. Fourier Transform Infrared Spectroscopy (FTIR) reveals that when moving from the biomass to the AC, there is a decomposition of several surface chemical function.

Keywords: *Activated carbon; Balanites aegyptiaca; Specific surface area*

1. Introduction

Activated carbons are carbonaceous materials used in various fields due to their high specific surface area and well-developed porosity. In recent years, the production of activated carbons has shifted from coal to biomass as raw materials because of its availability, low cost, and sustainability (Tung WoeyChew *et al.*, 2023; Haoufazane *et al.*, 2025). Two main methods are used to produce activated carbon from biomass: chemical and physical activation. Physical activation involves thermally decomposing the precursor in the absence of an oxidizing agent, then carbonizing the resulting residue with a gas such as carbon dioxide or moisture to activate it and obtain an extensive surface area and established porous structure. This procedure is normally carried out under controlled conditions at temperatures ranging from 600 to 1000 °C (Bansal *et al.*, 2005). Chemical activation, on the other hand, involves impregnating the biomass precursor with a chemical agent, usually a basic or acidic substance, followed by thermal decomposition of the precursor under strictly controlled conditions. A

structure with an enormous surface area and a clearly established pore diameter variation is created as a result of this procedure (Marsh & Reinoso, 2006). Our work aims to evaluate the effect of the activating agent on the specific surface area, porosity, morphology, and surface chemical functions of activated carbons produced from the trunk of Balanites aegyptiaca. Balanites aegyptiaca (BA), the desert date palm or date palm, is a tree belonging to the Balanitaceae family. The tree can reach a height of 10 meters, is highly branched, and thorny (with thorns up to 7 cm long). Its bark is striated, and its leaves are alternate, bifoliate, and approximately 5 cm long and 4 cm wide. Its flowers are greenish, and its fruits are ovoid drupes, 3 to 4 cm long, very angular, greenish during ripening, and light yellow when mature (Rongead, 2014). Furthermore, the physicochemical properties of activated carbons give them a very wide range of applications in diverse fields such as metallurgy, energy, the environment, etc. (Nuñez-Vargas *et al.*, 2026) material characterization techniques have been developed over the decades. These techniques can provide valuable information, and their selection depends on the nature of the material, the available analytical equipment, and the specific properties to be (El Meziani *et al.*, 2025).

2 Materials and methods

2.1 ATG/ATD Analysis

The thermochemical characteristics of Balanites aegyptiaca trunk (TBA) and of the prepared activated carbons (CAEs) were determined by thermogravimetry (PerkinElmer type, TGA 4000, Netherlands) carried out between 30 and 950 °C under a nitrogen (N_2) atmosphere with a heating rate of 10 °C/min.

2.2 Surface chemical functions

The method adopted for determining these functional groups is that of Boehm (1966). Basic groups are titrated as a whole, while acidic groups are titrated separately. The protocol is derived from the work of Omer (Nuñez-Vargas *et al.*, 2026). A mass of 0.2 g of CA was mixed with 20 of NaOH, Na_2CO_3, $NaHCO_3$, C_2H_5ONa, and (0.10 M) HCl in a series of 100 mL beakers. The beakers were sealed and shaken for 24 hours. After filtering the mixtures, 10 mL of each filtrate was pipetted, and the excess base or acid was titrated with a 0.10 M HCl or NaOH solution, using three drops of bromothymol blue (BBT), phenolphthalein, methyl red, methyl orange, and BBT, respectively.

2.3 FT-IR Spectroscopy

The surface chemical functions of the processed activated carbons and biomass (TBA) were quantified by Fourier Transform Infrared (FTIR) spectroscopy. The instrument used was an Agilent Technology Cary 630 FTIR. The spectrum was obtained over the frequency range from 650 to 4000 cm^{-1}.

2.4 Scanning electron microscopy coupled with energy-dispersive spectroscopy (SEM/EDS)

SEM coupled with EDS was used to study the surface morphology of the precursor and activated carbon, as well as the chemical composition of the elements. The instrument used was a ZEISS Gemini SEM. 1. Observations were carried out at different resolutions, including 10, 40 and 200 µm.

3 2.5 Textural analysis

The adsorption-desorption of (N_2) was used to determine the specific surface area, pore volume, and pore size distribution of the prepared samples (raw biomass, impregnated non pyrolyzed biomass, pyrolyzed raw biomass, and CAE-BA-25%-450°C). The experiments were performed at 77 K using

Quantachrome. NovaWin 4000e. The specific surface area was calculated using the Brunauer, Emmett , and Teller (BET) (Brunauer *et al.*, 1938), Langmuir, BJH, DH, t-plot, DR, and DFT methods. The total pore volume (Vtot) was determined by considering the amount of N_2 adsorbed at relative pressure (P/P°). The mesoporous volume was the difference between the total volume and the micropore volume. The mean pore diameter (dp) was obtained using the equation (**Eqn.1**):

$$\text{Eqn. 1. } d_p = \frac{4V_{tot}}{S_{BET}} \qquad \textbf{Eqn.1}$$

3 Results and discussion

3.1 TGA/DSC Analysis

The thermochemical behavior of the biomass used and the activated carbon was studied by TGA/DSC analysis. **Figure 1a-b,** presents the results of the thermal analysis of raw activated carbon (BA1) and activated carbon-25% at 450°C (BA5), respectively. The analysis of the TGA and DSC curves of raw activated carbon reveals three stages of degradation, characteristic of lignocellulosic biomass. These are: a first mass loss of 2.92% between 30 and 150°C, corresponding to the dehydration of the biomass; a second loss of 84.16% between 200 and 450°C, attributable to the removal of volatile matter and tar (hemicellulose and cellulose) (SANDA MAMANE Ousmaila, 2019) and a third loss of 3.95% above 450°C, corresponding to the slow degradation of lignin. Analysis of the CAE-BA-25%-450°C thermogram reveals greater thermal stability than raw BA.

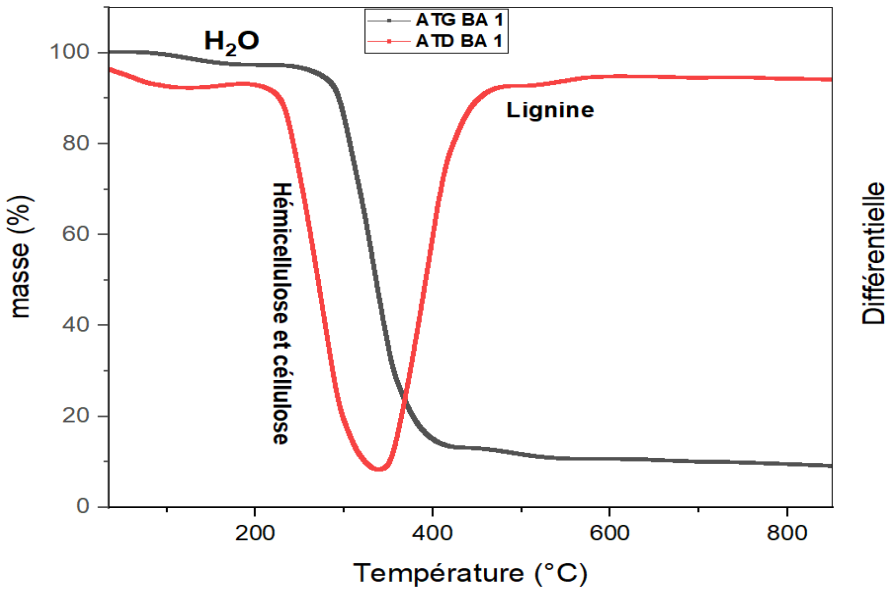

Figure 1a. Results of the thermal analysis of raw activated carbon (BA1)

A mass loss of 2.73% is observed between 30 and 100°C, corresponding to the elimination of physisorbed water. The primary decomposition, resulting in mass losses of 73.49%, begins at 350°C and reaches its maximum rate at 550°C. Comparison of the thermograms shows that raw BA is less thermally stable and rich in volatile matter, while CAE-BA-25%-450°C exhibits a more stable carbon structure than raw BA, with a single decomposition process. These observations confirm the successful activation and carbonization of the biomass. These results are consistent with the literature on CAs derived from plant biomass, as seen in the work of SANDA (2019), BEHLOUL (2023), and Elie (2023) (Elie SOGBOCHI, 2023; Mr. BEHLOUL Hamza, 2023; SANDA MAMANE Ousmaila, 2019).

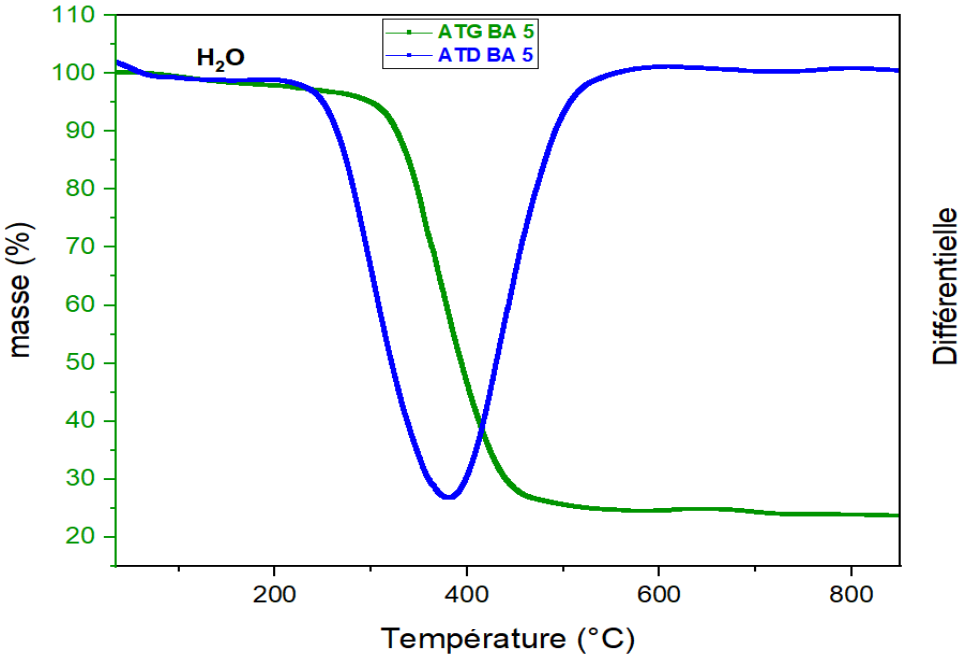

Figure 1b. Results of the thermal analysis of activated carbon-25% at 450°C (BA5)

3.2 Surface chemical functions

Chemical activation always generates chemical functionalities on the surface of activated carbon. **Table 1,** shows the results obtained for the surface functionalities in mEq/g of four prepared activated carbons.

Table 1. surface functionalities in mEq/g of four prepared activated carbons

Activated carbon	Carboxylic	Lactone	Phenol	Carbonyl	Total acid	Total basic
CAE-BA-20%-450°C	0.84	0.37	0.115	1.2	2.525	0.52
CAE-BA-25%-450°C	0.92	0.2	0.21	1.42	2.75	0.35
CAE-BA-30%-450°C	1.32	0.52	0.57	1.32	3.73	1.01
CAE-BA-25%-450°C-8h	1.01	0.13	0.24	1.45	2.83	0.96

These results show that the prepared activated carbons contain more acidic than basic functional groups. According to (Muhammad Hadzirun Muhamad Zubir & Muhammad Abbas Ahmad Zaini, 2020), the presence of basic functional groups in activated carbons chemically activated with orthophosphoric acid could originate from anionic phosphate mineral compounds present on the surface, if no chemical gasification agent is added during pyrolysis.

3.3 Fourier transform infrared (FT-IR) spectroscopy

The FT-IR spectra of raw BA (BA 1) and CAE-BA-25%-400°C are shown in **Figure 2a-b**, respectively. Figures 4 and 5 show characteristic bands of the chemical functional groups of raw BA and CAE-BA-25%-400°C (BA 13). **Figure 2a-b,** show that the wavenumbers generally decrease from raw BA to CAE-BA-25%-400°C, for example, from 3332 to 3278-2987 cm^{-1} for OH/NH. New bands

and peaks also appear on the CAE-BA-25% 400°C spectrum at 2655 cm^{-1} (P-OH) and 1276-1099 cm^{-1} (P-O or P-O-C), respectively. Some bands disappear when switching from biomass to CAE. Furthermore, transmittance values drop sharply after treatment of raw BA for all peaks and bands. This could be explained by the fact that the transfer of raw BA to activated carbon decomposes certain functional groups (Adam & Al-Shammari, 2023; Guessoum Kaouthar, 2020; Maâzou Siragi D. B. *et al.*, 2025).

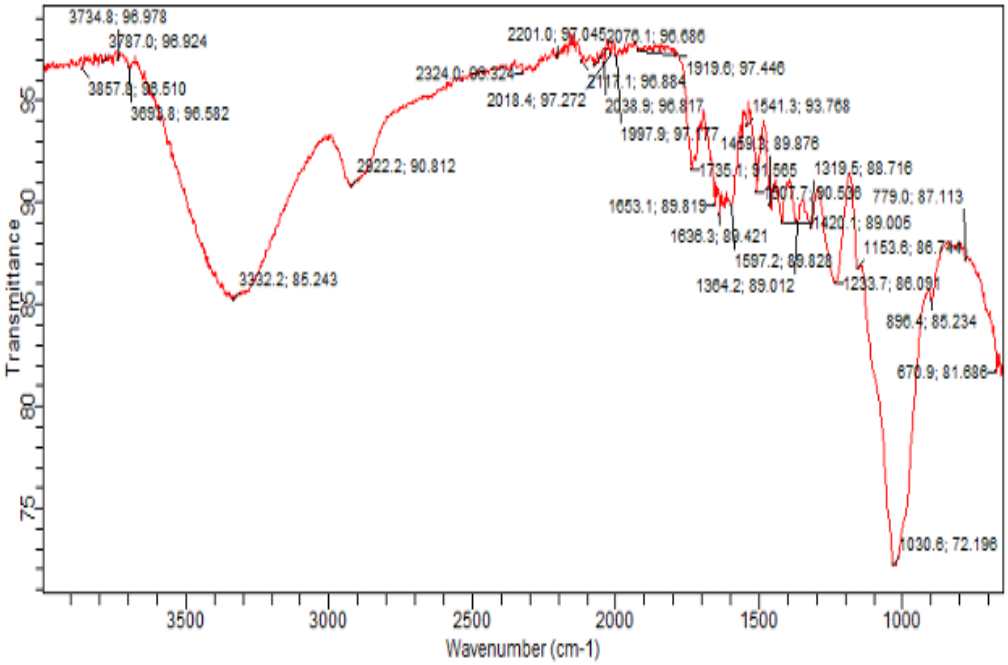

Figure 2a. Infrared Spectrum of Raw BA (BA1)

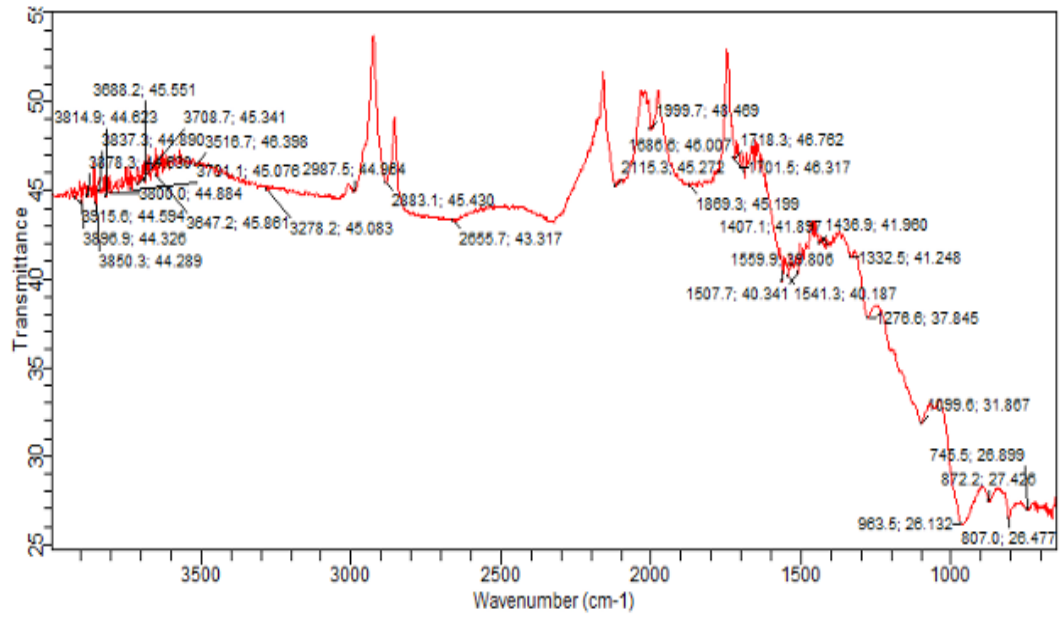

Figure 2b. Infrared Spectrum of CAE-BA-25%-400°C (BA13)

3.4 Scanning electron microscopy coupled with energy-dispersive spectroscopy (SEM/EDS)

SEM was performed on raw BA and CAE-BA-20%-450°C to observe the activation effect. **Figures 3** and **4,** show the images and EDS diagrams of raw BA and CAE-BA-20% 450°C, respectively. SEM

observations of raw BA and CAE-BA-20%-450°C at different resolutions show that raw BA (**Figure 3**) is in fibrous form and its external surface is less rough. In contrast, mixed porosity is observed across the entire surface of the activated carbon (**Figure 4**). This explains why orthophosphoric acid activation created pores within the biomass. This is confirmed by the literature (Mahamane Nassirou A. K., *et al.*, 2022; Mr. BEHLOUL Hamza, 2023; SANDA MAMANE Ousmaila, 2019).

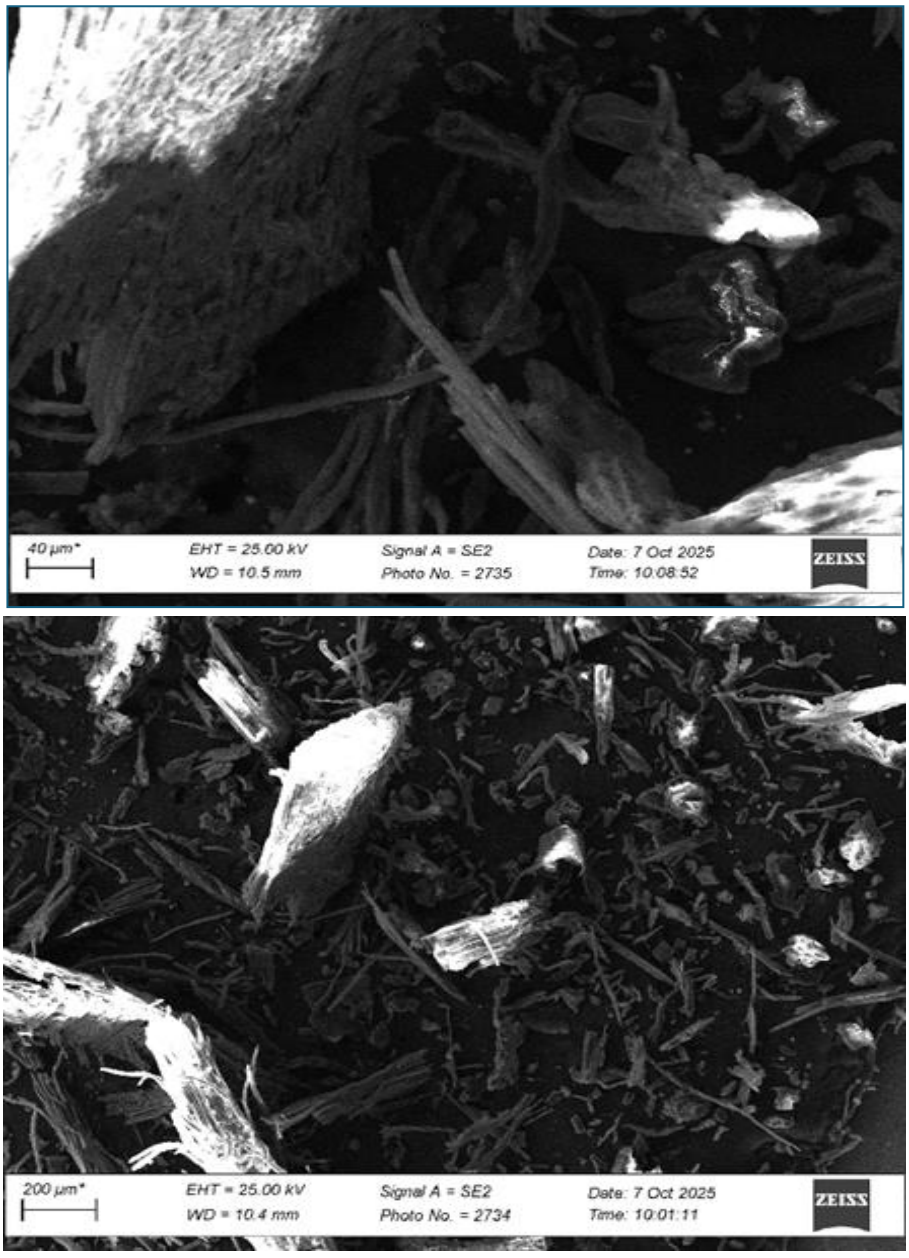

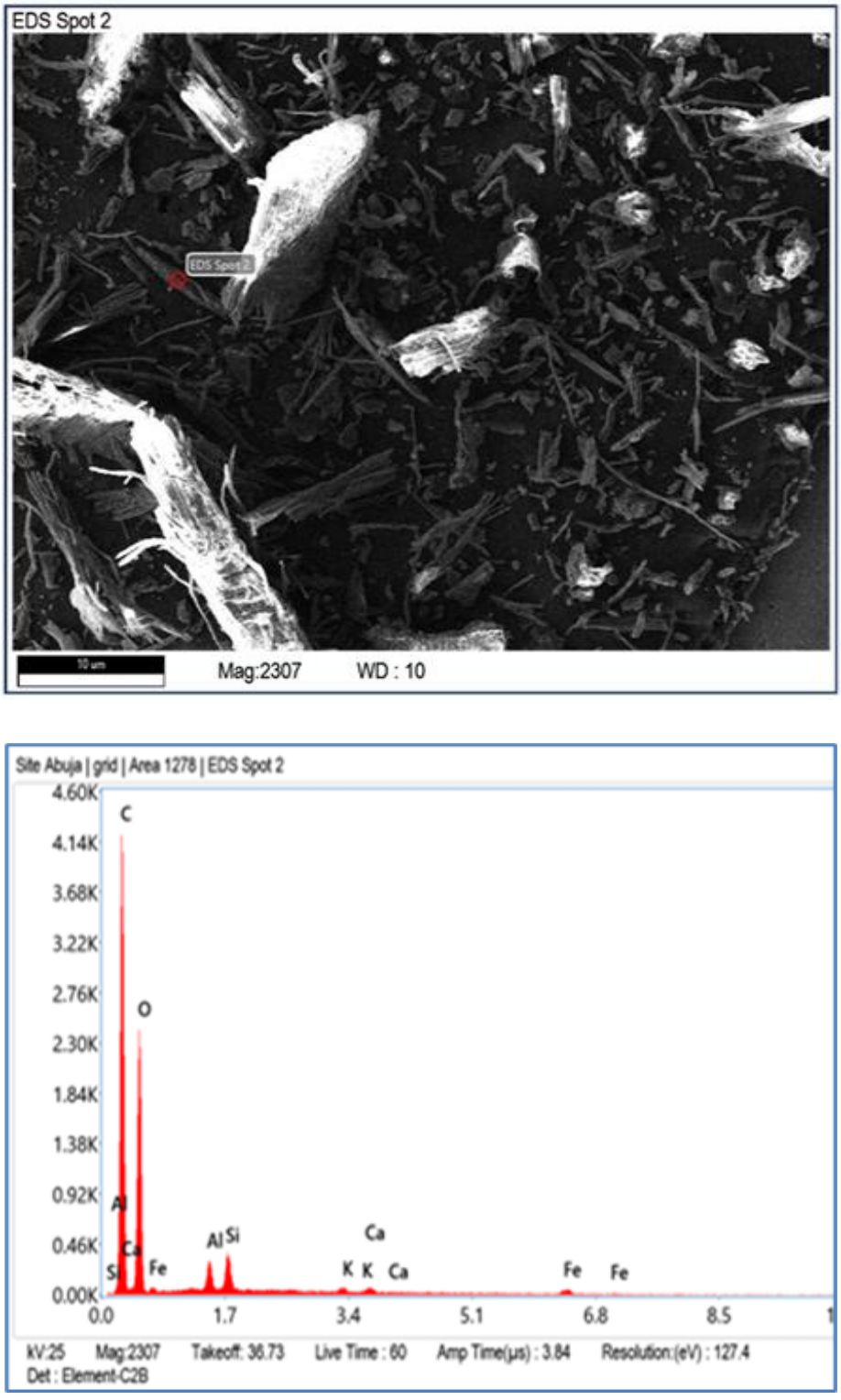

Figure 3. Scanning electron microscopy coupled with energy-dispersive spectroscopy of BA-brute (BA1)

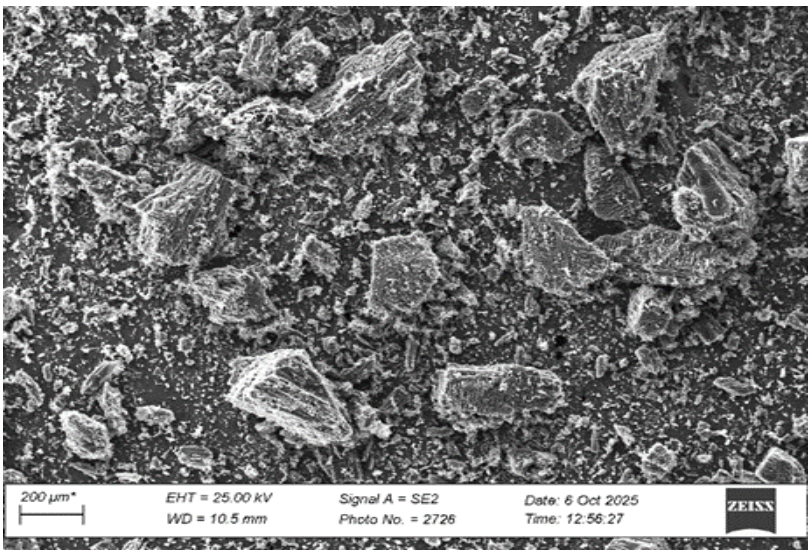
200 µm*
EHT = 25.00 kV
WD = 10.5 mm
Signal A = SE2
Photo No. = 2726
Date: 6 Oct 2025
Time: 12:56:27
ZEISS

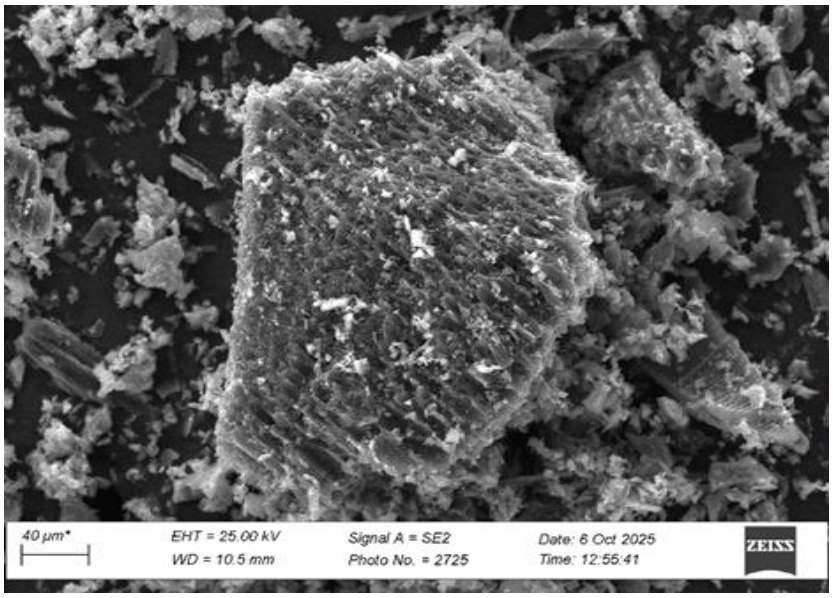
40 µm*
EHT = 25.00 kV
WD = 10.5 mm
Signal A = SE2
Photo No. = 2725
Date: 6 Oct 2025
Time: 12:55:41
ZEISS

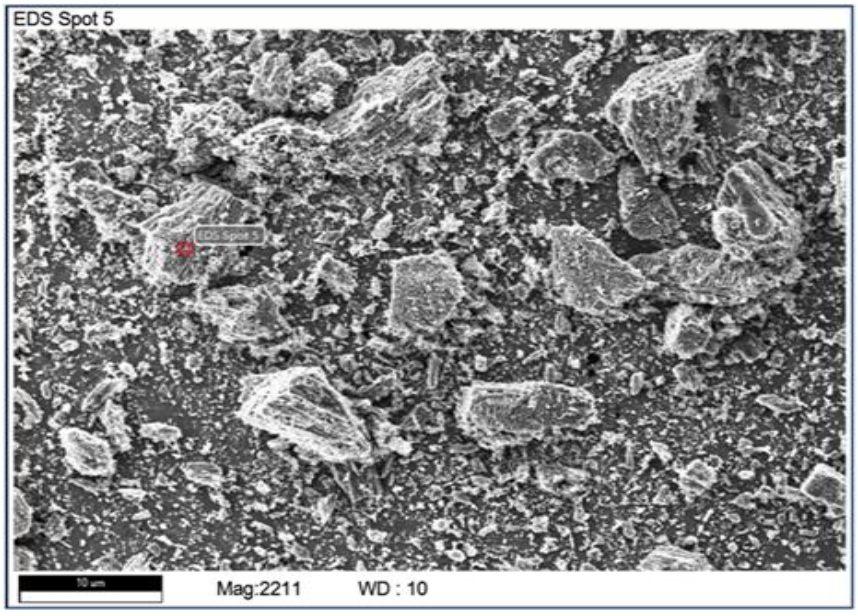
EDS Spot 5
Mag:2211
WD : 10

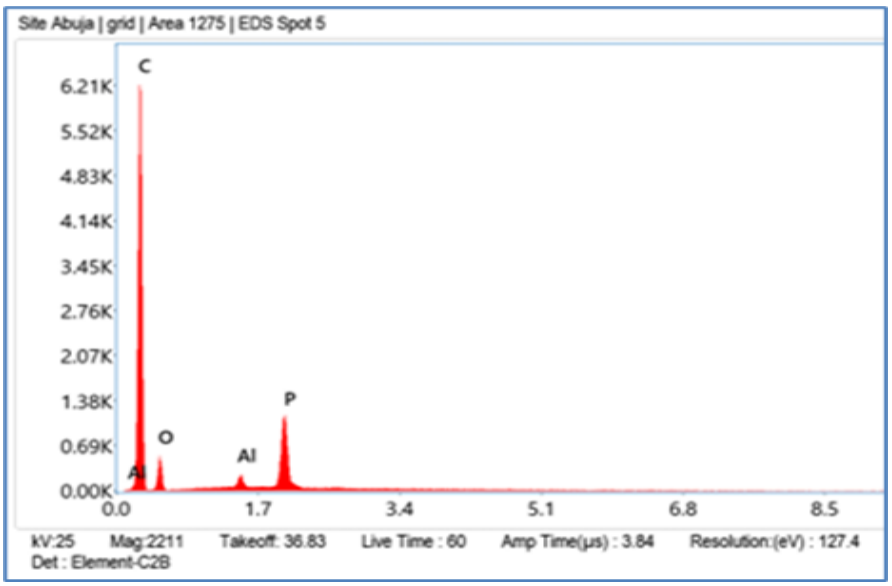

Figure 4. Scanning electron microscopy coupled with energy-dispersive spectroscopy of CAE-BA-20%-450°C

The results of the EDS analysis of raw BA and CAE-BA-20%-450°C are illustrated in **Table 2**. EDS analyses show an increase in carbon content from 71.89% to 91.28%, while the oxygen content decreases from 27.56% to 7.89% when transferring from biomass to activated carbon. This variation may be due to the carbonization process, which induces decarboxylation and dehydration of the biomass, thus promoting the high carbon content. The phosphorus detected by EDS originates from the residual activator (H_3PO_4 after washing the activated carbon (Sivaranjanee *et al.*, 2024). The carbon content of the prepared activated carbon is higher than that found by Kiari *et al.*, on HT - based activated carbon. who found a value of 71.90% (Mahamane Nassirou A. K., *et al.*, 2022).

Table 2. Results of the EDS analysis of raw BA and CAE-BA-20%-450°C

Elements	Mass percentage (%)		Atomic percentage (%)	
	BA-Brute	CAE-BA-20%-450°C	BA-Brute	CAE-BA-20%-450°C
CK	65.32	87.86	71.89	91.28
OK	33.36	10.12	27.56	7.89
Al K	0.44	0.31	0.22	0.14
If K	0.47	-	0.22	-
K K	0.08	-	0.03	-
Ca K	0.1	-	0.03	-
Fe K	0.22	-	0.05	-
PK	-	1.72	-	0.69

3.5 Textural analysis

3.5.1 Specific surface areas determined by different methods

Table 3, shows the specific surface areas obtained by different methods. The results presented in **Table 3,** show that the different methods used to determine the specific surfaces of our samples are complementary and describe: the total accessible surface (BET, Langmuir), the micro/mesoporous

distribution (BJH, DH, t-plot and DR), and the effective surface at the nanometric scale (DFT). Thus, raw BA exhibits a specific surface area (BET) of 173.1 m²/g, which explains its dense structure and limited N_2 accessibility Indeed, impregnation slightly increases the BET surface area (196.6 m²/g), but pyrolysis of raw BA significantly increases both the BET surface area (218.2 m²/g) and the microporous surface area determined by the Dubinin Radushkevich method (243.8 m²/ g). This change could be attributed to the removal of volatile matter following thermal decomposition. These results are similar to those found by Lua and Yang, who reported a similar increase in specific surface area after carbonization of plant biomass (Lua & Yang, 2004).

Table 3. Specific surface areas (m^2/g) of the samples

Specific surface area (m^2 / g)	BA-brute	Non-pyrolyzed impregnated BA	BA-brute pyrolyzed	CAE-BA-25%-450°C	CAE-BA-25%-450°C-16h
BET at a single point	133.8	117.3	143.2	-	310.3
BET multipoint	173.1	196.6	218.2	282,614	393.6
Langmuir	404	1406	776.8	986,585	880.2
BJH	229.4	218	263.1	349,978	509.5
DH	245.3	232	281.7	-	543.4
t -plot	173.1	196.6	218.2	282,614	393.6
DR	215.5	207.8	243.8	323,782	500.7
DFT	55.14	45.88	57.46	76,208	133.2

Chemical activation at 25% followed by pyrolysis at 450°C significantly improved all specific surface areas. The BJH surface area increased from 229.4 m²/g for raw BA to 509.5 m²/g for CAE-BA-25%-450°C-16h. The Langmuir surface areas of all samples were high, ranging from 404 to 1406 m²/g, exceeding those of BET. CAE-BA-25%-450°C-16h exhibits the highest values for all characterization methods, with a multipoint BET area of 393.6 m²/g, a DR microporous area of 500.7 m²/g and a BJH area of 509.5 m²/g.

3.5.2 Pore volumes of samples determined by different methods

Table 4, shows the pore volumes of the samples obtained by different methods.

Table 4. Pore volume (cm^3/g) of the samples

Pore volume (cc/g)	BA-brute	Non-pyrolyzed impregnated BA	BA-brute pyrolyzed	CAE-BA-25%-450°C	CAE-BA-25%-450°C-16h
BJH	0.1104	0.1074	0.1265	0.171	0.2459
DH	0.1133	0.1099	0.13	-	0.2519
DR	0.07657	0.07386	0.08664	0.115	0.1779
HK	0.03916	0.03037	0.03919	-	0.09275
SF	0.01341	0.005934	0.009685	-	0.03479
DFT	0.06333	0.05558	0.06834	0.091	0.1473

The cumulative pore volumes obtained by the BJH and DH methods increased from (0.1104; 0.1133 cm³/g) to (≈ 0.25 cm³/g) from BA-Brute to CAE-BA-25%-450°C-16h. This trend was confirmed by the DFT method, with a total pore volume reaching 0.1473 cm³/g for the most activated sample (Rouquerol *et al.*, 2013a). Thus, the development of microporosity is estimated by the methods (DR,

HK and SF) which show an increase in microporous volumes from 0.005934 to 0.1779 cm3/g. According to Dubinin, this type of microporosity is directly correlated with a high capacity for adsorption of gases and small dissolved pollutants (E. M. Dubinin, & L. Radushkevich, 1947).

3.5.3 Pore diameters of samples determined by different methods

Table 5, shows the diameters of the samples obtained by different methods.

Table 5. Pore diameters (nm) of the samples

Pore diameter (nm)	BA-brute	Non-pyrolyzed impregnated BA	BA-brute pyrolyzed	CAE-BA-25%-450°C	CAE-BA-25%-450°C-16h
BJH	2,433	2.102	2.103	2,129	2,423
DH	2,433	2.102	2.103	2,129	2,423
DR	5,349	6,315	5,901	5,903	5,283
DA	2.68	2.96	2.86	2.86	2.64
HK	3.675	1,847	1,847	-	3.675
SF	4,523	3,414	4,523	-	4,523
DFT	2,647	2,647	2,647	2,647	2,647

In general, pore diameters obtained by different methods range from 1.847 to 6.315 nm. Thus, the values obtained with BJH and DH are the same for each sample. Furthermore, the cumulative pore diameters obtained by the DFT method are identical (2.647) for all samples. This confirms the reliability of this method for CA, as it covers the entire micro-mesoporous scale well. The highest pore diameter values (> 5 nm) are obtained by the Dubinin method. Radushkevich. However, the diameters obtained with CAE-BA-25% 450°C-16h are almost identical to those of BA-Brute.

3.5.4 Correlation coefficients and constants for different techniques

Table 6, shows the correlation coefficients (R^2) and constants (C) obtained for the BET, Langmuir and DR methods.

Table 6. Correlation coefficients and constants for different techniques

	Method of analysis			
	BET		Langmuir	DR method
Samples	C	R^2	R^2	
BA-brute	7,183	0.991789	0.939	0.9819
Non-pyrolyzed impregnated BA	3,287	0.998331	0.861	0.9891
BA-brute pyrolyzed	4,378	0.992111	0.898	0.9865
CAE-BA-25%-450°C	4.54	0.994476	0.914	0.9872
CAE-BA-25%-450°C-16h	7,898	0.992589	0.946	0.9811

The very good fits of the BET and Dubinin – Radushkevich models ($R^2 > 0.98$) indicate that adsorption is dominated by multilayer adsorption and micropore filling, consistent with the high BET and DR

areas obtained after pyrolysis and activation. The increase in the (7.898) BET constant, which is maximal for the CAE-BA-25%-450°C-16h sample, reflects a strengthening of adsorbate–adsorbent interactions. Conversely, the poor fit of the Langmuir model confirms that adsorption is not limited to a monolayer on a homogeneous surface, which is consistent with the pore heterogeneity revealed by BJH analysis (Rouquerol *et al.*, 2013b).

Conclusion

TGA/DTA analysis reveals that biomass exhibits lower thermal stable than the prepared activated carbons. Impregnation slightly alters the structure and morphology of the biomass. Impregnation followed by pyrolysis significantly increases the specific surface area of the prepared activated carbons for all methods used. Pyrolysis alone significantly increases the specific surface area of both unimpregnated and orthophosphoric acid-impregnated biomass. Pyrolysis increases specific surface area more effectively than impregnation alone. The activated carbon that developed the highest specific surface area (393.6 m²/g) was CAE-BA-25%-450°C-16h.

Acknowledgement, we extend our sincere thanks to the staff of the Materials, Water and Environment Laboratory of the Department of Chemistry, Faculty of Science and Technology, Abdou Moumouni University of Niamey.

Disclosure statement: *Conflict of Interest:* The authors declare that there are no conflicts of interest.

Compliance with Ethical Standards: This article does not contain any studies involving human or animal subjects.

References

Adam, O. E.-A. A., & Al-Shammari, A. S. (2023) Preparation and characterization of activated carbon from Balanites aegyptiaca seed shell for the removal of 2,4-dichlorophenoxyacetic acid herbicide from aqueous solution. *Desalination and Water Treatment*, *315*, 314-326. https://doi.org/10.5004/dwt.2023.30138

Bansal, R. C., Goyal, M., Bansal, R. C., & Goyal, M. (2005) *Activated Carbon Adsorption Activated Carbon Adsorption*.

Brunauer, S., Emmett, P. H., Teller, E. (1938) Adsorption of Gases in Multimolecular Layers. *Journal of the American Chemical Society*, *60*(2), 309-319. https://doi.org/10.1021/ja01269a023

Dubinin E. M., & L. Radushkevich. (1947) *Equation of the Characteristic Curve of Activated Charcoal –ScienceOpen*. https://www.scienceopen.com/document?vid=b88870c5-c14a-4571-b5aa-54e720ac5b54

El Meziani, S., Agnaou, H., El Haddaj, H., Boumya, W., Barka, N., & Elhalil, A. (2025) Sustainable adsorption technologies for textile dye removal: Advances in biomass-derived and magnetically modified activated carbons. *Cleaner Chemical Engineering*, *12*, 100210. https://doi.org/10.1016/j.clce.2025.100210

Elie SOGBOCHI. (2023) *Elaboration par voies thermochimiques de charbons actifs dérivés de coproduits de Lophira lanceolata : Essais d'adsorption de micropolluants de l'eau*. Thèse de Doctorat, Universite d'Abomey-Calavi (UAC/Benin) et Universite de Lorraine (UL/France).

Guessoum Kaouthar. (2020) *Élimination du nickel (II)à base de noix d'olives* [Mémoire] de master, Université de Biskra, Algérie.

Haoufazane, C., Zaaboul, F., Monfalouti, H.E., Jodeh S., Azzaoui K., Hammouti B., Tihmmou R., Salghi R. & Kartah B.E. (2025). Enhanced removal of C.I. direct black 80 by phosphoric acid

activated plant biomass supported by DFT insights. *Sci Rep* 15, 40134 https://doi.org/10.1038/s41598-025-23886-z

Lua, A. C., & Yang, T. (2004) Effect of activation temperature on the textural and chemical properties of potassium hydroxide activated carbon prepared from pistachio-nut shell. *Journal of Colloid and Interface Science*. https://doi.org/10.1016/j.jcis.2003.10.001

Maâzou Siragi D. B., Halidou I. Hima, Ibrahim Natatou, & Vincent Dubois. (2025) A comparative study of the adsorption kinetics of $AuCN_2^-$ and $AuS_2O_32_3^-$ by prepared activated carbon. *Results in Chemistry*, *17*, 102641. https://doi.org/10.1016/j.rechem.2025.102641

Mahamane Nassirou A. K., Guy Didier F., Affoué Tindo Sylvie K., Adama O., Horo K., Maman Mousbaou M. A., Emmanue Nogbou A., & Kouassi Benjamin Y. (2022) *Process conditions optimization of plant waste-derived microporous activated carbon using a full factorial design and genetic algorithm*. *Journal of Materials and Environmental Science*, 13, Issue 8, 884-899.

Marsh, H., & Reinoso, F. R. (2006) *Activated Carbon*. Elsevier Science. https://www.perlego.com/book/1835563/activated-carbon-pdf

Mr. BEHLOUL Hamza. (2023). *Synthèse et caractérisation de nouveaux matériaux : Application dans le domaine de la dépollution des eaux*. Mohamed El Bachir El Ibrahimi Bordj Bou Arreridj.

Muhammad Hadzirun Muhamad Zubir & Muhammad Abbas Ahmad Zaini. (2020) *Twigs-derived activated carbons via $H_3PO_4/ZnCl_2$ composite activation for methylene blue and congo red dyes removal | Scientific Reports*. https://doi.org/doi.org/10.1038/s41598-020-71034-6

Nuñez-Vargas, D., Barraza-Burgos, J., Guerrero-Perez, J., Diaz, L., Dalai, A. K., & Borugadda, V. B. (2026) Oil Palm Shell-Derived Activated Carbon: Adsorption Kinetics, Thermodynamics, and Interaction Mechanism for Lufenuron 50-EC Pesticide. *ACS Omega*.

Rongead. (2014) *Balanites_aegyptiaca_16.09*. (s. d.).

Rouquerol, J., Rouquerol, F., Llewellyn, P., Maurin, G., & Sing, K. (2013a). *Adsorption by Powders and Porous Solids: Principles, Methodology and Applications*. Academic Press.

Rouquerol, J., Rouquerol, F., Llewellyn, P., Maurin, G., & Sing, K. (2013b) *Adsorption by Powders and Porous Solids: Principles, Methodology and Applications*. Academic Press.

SANDA MAMANE Ousmaila. (2019) *Valorisation de déchets agro-alimentaires pour l'élaboration de charbons actifs ; caractérisation et application dans la dépollution des eaux usées chargées en chrome issues de la Tannerie Malam Yaro de Zinder-Niger*. Thèse de Doctorat, Université Abdou Moumouni de Niamey, Niger.

Sivaranjanee, R., Kumar, P. S., & Rangasamy, G. (2024) Hydrothermally produced activated carbon spheres from discarded maize cobs for efficient removal of rose bengal dye from water environment. *Desalination and Water Treatment*, *317*, 100123. https://doi.org/10.1016/j.dwt.2024.100123

Tung WoeyChew, Paik San H'Ng, Bin Chuah Teong Guan Luqman Chuah Abdullah, Kit Ling Chin, Chuan Li Lee, Bin MohdSahfani MohdNorHafizuddin, & LuluTaungMai. (2023) *AReviewofBio-Based Activated Carbon Properties Produced from Different Activating Chemicals during Chemicals Activation Process on Biomass and Its Potential for Malaysia*. 15. https://doi.org/10.3390/ma16237365